Theoretical and Experimental Studies of the Photoluminescent Properties of the Coordination Polymer [Eu(DPA)(HDPA)(H 2 O) 2]·4H 2 O

ARTICLE *in* THE JOURNAL OF PHYSICAL CHEMISTRY B · MAY 2008

Impact Factor: 3.3 · DOI: 10.1021/jp075047m · Source: PubMed

9 AUTHORS, INCLUDING:

Carlos Alberto de Simone
University of São Paulo
123 PUBLICATIONS **863** CITATIONS
SEE PROFILE

Antonio M. Brito-Silva
University of Victoria
18 PUBLICATIONS **336** CITATIONS
SEE PROFILE

Severino Alves
Federal University of Pernambuco
129 PUBLICATIONS **1,548** CITATIONS
SEE PROFILE

Ricardo Oliveira Freire
Universidade Federal de Sergipe
85 PUBLICATIONS **1,900** CITATIONS
SEE PROFILE

Theoretical and Experimental Studies of the Photoluminescent Properties of the Coordination Polymer $[Eu(DPA)(HDPA)(H_2O)_2]\cdot 4H_2O$

Marcelo O. Rodrigues,*,† Nivan B. da Costa Júnior,‡ Carlos A. de Simone,§ Adriano A. S. Araújo,‡ A. M. Brito-Silva,|| Filipe A. Almeida Paz,⊥ Maria E. de Mesquita,‡ Severino A. Júnior,*,† and Ricardo O. Freire*,‡

Departamento de Química Fundamental, UFPE, 50590-470, Recife - PE, Brazil, Departamento de Química, UFS, 49100-000, São Cristóvão - SE, Brazil, Departamento de Química, UFAL, 57072-970, Maceió - AL, Brazil, Pós-Graduação em Ciência de Materiais, UFPE, 50590-470, Recife - PE, Brazil, Departamento de Química, CICECO, Universidade de Aveiro, 3810-193, Aveiro, Portugal

Received: June 28, 2007; In Final Form: December 4, 2007

We report on the hydrothermal synthesis of the $[Eu(DPA)(HDPA)(H_2O)_2]\cdot 4H_2O$ lanthanide-organic framework (where H_2DPA stands for pyridine-2,6-dicarboxylic acid), its full structural characterization including single-crystal X-ray diffraction and vibrational spectroscopy studies, plus detailed investigations on the experimental and predicted (using the Sparkle/PM3 model) photophysical luminescent properties. We demonstrate that the Sparkle/PM3 model arises as a valid and efficient alternative to the simulation and prediction of the photoluminescent properties of lanthanide-organic frameworks when compared with methods traditionally used. Crystallographic investigations showed that the material is composed of neutral one-dimensional coordination polymers $_{\infty}^{1}[Eu(DPA)(HDPA)(H_2O)_2]$ which are interconnected via a series of hydrogen bonding interactions involving the water molecules (both coordinated and located in the interstitial spaces of the structure). In particular, connections between bilayer arrangements of $_{\infty}^{1}[Eu(DPA)(HDPA)(H_2O)_2]$ are assured by a centrosymmetric hexameric water cluster. The presence of this large number of O−H oscillators intensifies the vibronic coupling with water molecules and, as a consequence, increases the number of nonradiative decay pathways controlling the relaxation process, ultimately considerably reducing the quantum efficiency ($\eta = 12.7\%$). The intensity parameters (Ω_2, Ω_4, and Ω_6) were first calculated by using both the X-ray and the Sparkle/PM3 structures and were then used to calculate the rates of energy transfer (W_{ET}) and back-transfer (W_{BT}). Intensity parameters were used to predict the radiative decay rate. The calculated quantum yield obtained from the X-ray and Sparkle/PM3 structures (both of about 12.5%) are in good agreement with the experimental value ($12.0 \pm 5\%$). These results clearly attest for the efficacy of the theoretical models employed in all calculations and create open new interesting possibilities for the design in silico of novel and highly efficient lanthanide-organic frameworks.

Introduction

The use of lanthanide ions in the construction of coordination polymers, also known as metal−organic frameworks (MOFs), has recently received much attention,[1−3] since the intrinsic magnetic and photoluminescence (PL) properties of these materials render them as potential candidates for the development of functional devices.[4−6] In particular, these framework-based materials can efficiently be used in light conversion molecular devices (LCMD),[7] in which light is absorbed by the coordinated ligands and then transferred to the emitting metal ion, ultimately increasing the overall PL properties.[8] Europium-based systems are of particular interest because they usually have long lifetimes and quantum efficiencies.[9] In addition, the Eu^{3+} (4f−4f) transitions are particularly sensitive to the coordination modes of the organic ligands and, therefore, can be efficiently used to infer structural features of individual coordination environments.[10] These photophysical characteristics have been extensively explored in materials science, in particular, in the development of luminescent probes in biomedical assay,[11] organic light-emitting diodes (OLEDs),[12] and sensors.[13]

A great diversity of organic ligands have been strategically developed and used on the synthesis of new europium complexes, among which the pyridinecarboxylate-based molecules are of particular interest due to their chemical stability and photophysical properties.[14−15] For example, pyridine 2,6-dicarboxylic acid (H_2DPA) has been widely employed on the preparation of complexes with Eu^{3+} cations which find applications in biological systems and immunoassays.[16−17] Moreover, H_2DPA also plays a decisive role on the construction of coordination polymers since it can establish bridges between metals centers and adopt several coordination modes.[18] It is important to emphasize that, even though a number of reports on the synthesis of MOFs with Eu^{3+} and H_2DPA residues are available in the literature, a detailed study of the PL properties of these compounds is, to date, nonexistent.[19−20]

In silico methods are nowadays particularly efficient addressing interesting chemical problems associated with structure prediction and anticipation of photophysical properties.[21] For

* Corresponding authors. E-mail: mzohio@hotmail.com (M.O.R.), salvesjr@ufpe.br (S.A.J.), and rfreire@ufs.br (R.O.F.).
† Departmento de Química Fundamental, UFPE.
‡ UFS.
§ UFAL.
|| Pós-Graduação em Ciência de Materiais, UFPE.
⊥ CICECO.

10.1021/jp075047m CCC: $40.75
Published on Web 03/18/2008 PAGE EST: 8.4

example, quantum chemical methods are able to calculate the ground state geometry of lanthanide centers, and first principles methods using effective core potentials (ECPs) have proven their effectiveness in lanthanide chemistry.[22−24] Nevertheless, these methodologies are computationally very demanding and, thus, inappropriate for expanded systems such as MOFs. Sparkle/AM1 algorithms[25] are instead based on a sophisticated parametrization scheme for semiempirical calculations, allowing the prediction of coordination geometries whose accuracy is comparable to those obtained from ab initio/ECP calculations but at much smaller expense of computational power.[25−26] The Sparkle/AM1 model has been successfully applied to the prediction of the ground state geometries of lanthanide complexes, the corresponding ligand field parameters,[27−29] plus a number of other spectroscopic properties such as electronic spectrum, singlet and triplet energy positions,[30−32] and intensity parameters.[33−35] By using the two latter series of calculated parameters, we have recently built up rate equations involving energy transfer mechanisms which allowed the determination of PL efficiencies and quantum yields,[36,37] and, in a more recent study, we have reported the design of a highly photoluminescent europium complex simply based on theoretical studies.[37]

In this paper, we report a detailed (theoretical and experimental) photophysical study of the properties of the one-dimensional coordination polymer, $[Eu(DPA)(HDPA)(H_2O)_2]\cdot 4H_2O$, recently described very briefly by Harrowfield and collaborators.[38] Spectroscopic properties such as intensity parameters Ω_λ ($\lambda = 2$, 4 and 6), rates of energy transfer (W_{ET}) and back-transfer (W_{BT}), branching ratios (β_{OJ}), radiative (A_{rad}) and nonradiative (A_{nrad}) decay rates, quantum efficiency (η), and quantum yield (q) of this material were theoretically predicted using the Sparkle/PM3 geometry and data derived from single-crystal X-ray diffraction investigations. We decided to use the Sparkle/PM3 parametrization[25] model since it has a better quantum chemical description of the coordinated ligands, which ultimately is reflected in the overall quality of the predicted PL properties.

Experimental Details

Synthesis of $Eu(DPA)(HDPA)(H_2O)_2]\cdot 4H_2O$. A mixture of pyridine-2,6-dicarboxylic acid, H_2DPA, (0.8 mmol, 0.134 g), Eu_2O_3 (0.070 g, 0.2 mmol), and H_2O (ca. 4 mL) was placed in a 8 mL Teflon-lined stainless autoclave at 180 °C for 72 h. The final compound (0.123 g) was obtained in a yield of ca. 60% (based on Eu) after being washed with water and acetone and being air-dried. Anal. calcd for $C_{14}H_{14}N_2O_{14}Eu$ (%): C, 28.68; H, 2.41; N, 4.78. Found (%): C, 27.38; H, 2.52; N, 4.90. IR (cm^{-1}): 3565−3065 (s), 1613 (s), 1566 (s), 1450 (s), 1395 (s), 1377 (s), 1284 (m), 1191 (w), 1076 (m), 1016 (w), 916 (w), 700 (m), 591 (w), 506 (w), 408 (w). The IR spectra (coordination polymer and H_2DPA ligand) are presented in Supporting Information (Figure S3).

General Instrumentation. Elemental analysis was performed on a CHNS−O analyzer Flash 1112 Series EA Thermo Finnigam. FT-IR spectra were recorded on KBr pellets (spectral range 4000 to 400 cm^{-1}) using a BRUKER IFS 66.

Photoluminescence spectra at room temperature and 77 K were obtained using a ISS PC1 spectrofluorometer. The excitation device was equipped with a 300 W xenon lamp and a holographic grating. Emission spectra were collected with a 25 cm monochromator (resolution of 0.1 nm) connected to a photomultiplier. The excitation and emission slit width were fixed at 1.0 mm, with all used monochromators having 1200 grooves/mm. The experimental quantum yield (q) was determined by employing the method developed by Bril et al.,[39] for which the q value for a give sample can be calculated by a direct comparison with standard phosphors whose q values were previously determined by absolute measurements. q can thus be determined by:

$$q = \left(\frac{1 - r_{ST}}{1 - r_x}\right)\left(\frac{\Delta\Phi_x}{\Delta\Phi_{ST}}\right)q_{ST} \quad (1)$$

where r_{ST} and r_x correspond to the amount of exciting radiation reflected by the standard and the sample, respectively, and q_{ST} is the quantum yield of the standard phosphor. The terms $\Delta\Phi_x$ and $\Delta\Phi_{ST}$ correspond to the respective integrate photon flux (photon·s^{-1}) for the sample and standard phosphors. As standard phosphor we used sodium salicylate (Merck PA), whose q_{ST} is 55% at room temperature as reported by Malta and co-workers.[40]

Differential scanning calorimetry (DSC) data was recorded in a DSC 50 cell (Shimadzu) in the 25−400 °C temperature range, under dynamic nitrogen atmosphere (50 mL·min^{-1}), and by using an aluminum crucible with ∼2.0 mg of the sample and a heating rate of 10 °C·min^{-1}. The DSC cell was calibrated with indium (mp 156.6 °C; ΔH_{fus} = 28.54 J·g^{-1}). The thermoanalytical curves were obtained in duplicate with a thermobalance model TGA 50 (Shimadzu) in 25−1200 °C temperature range, using a platinum crucible with approximately 3.0 mg of sample, under dynamic nitrogen atmosphere (50 mL·min^{-1}) and with a heating rate of 10 °C·min^{-1}.

Single-Crystal X-ray Diffraction. A detailed description of the crystallographic characterization of the compound is presented in Supporting Information.

Theoretical Studies

Geometry Optimization and Transition Energies. The Sparkle/PM3[25] model, implemented in the Mopac2007 software package,[41] was used to calculate the ground state geometry of the $[Eu(DPA)(HDPA)(H_2O)_2]\cdot 4H_2O$ compound. MOPAC keywords: PRECISE, GNORM= 0.25, SCFCRT = 1.D-10 (to increase the SCF convergence criterion) and XYZ (for Cartesian coordinates).

The X-ray and Sparkle/PM3 optimized geometries were used to calculate the singlet and triplet excited states using configuration interaction single (CIS) based on the intermediate neglect of differential overlap/spectroscopic (INDO/S) method[42−43] implemented in the ZINDO program.[44]

Judd-Ofelt Intensity Parameters Calculation. The experimental intensity parameters, Ω_λ, for $[Eu(DPA)(HDPA)(H_2O)_2]\cdot 4H_2O$ were determined from:

$$\Omega_\lambda = \frac{4e^2\omega^3 A_{0J}}{3\hbar\chi\langle {}^7F||U^\lambda||{}^5D_0\rangle^2} \quad (2)$$

where A_{0J} are the coefficient of spontaneous emission for the ${}^5D_0 \rightarrow {}^7F_J$ transition, χ is the Lorentz local-field correction term given by $\chi = n(n^2 + 2)^2/9$, n is the refractive index of the medium (in this case $n = 1.5$), and $|\langle {}^5D_0||U^{(\lambda)}||{}^7F_J\rangle|^2$ are the square reduced matrix element whose values are 0.0032, 0.0023, and 0.0002 for $\lambda = 2$, 4, and 6, respectively.[45,46] The transition ${}^5D_0 \rightarrow {}^7F_6$ is not observed experimentally thus the experimental Ω_6 parameter cannot be estimated.

The coordinative interaction between a lanthanide cation and a ligand L can be described by the Judd-Ofelt theory,[47−48] after which the intensity parameters Ω_λ ($\lambda = 2$, 4, and 6) are defined by:

$$\Omega_\lambda = (2\lambda + 1) \sum_{t,p} \frac{|B_{\lambda tp}|^2}{(2t + 1)} \quad (3)$$

with

$$B_{\lambda tp} = \frac{2}{\Delta E} \langle r^{t+1} \rangle \theta(t, p) \gamma t_p - \left[\frac{(\lambda + 1)(2\lambda + 3)}{2\lambda + 1} \right] \langle r^t \rangle (1 - \sigma_\lambda) \langle f \| C^{(\lambda)} \| f \rangle \Gamma^t_p \delta_{t,\lambda+1} \quad (4)$$

Details on the parameters of eqs 3 and 4 are widely discussed in the literature.[49−52]

The values of charge factors (g) and the polarizability of the ligand L (α) (Table 2) used for the calculation of γ^t_p and Γ^t_p, respectively, were adjusted using a nonlinear minimization of an eight-dimension response surface. The generate simulating annealing (GSA) method was employed in order to find one of its local minima, which ideally should be the global one and be chemically feasible. During the minimization stage, both the Sparkle/PM3 and the single-crystal X-ray diffraction geometries were used. The response function, F_{resp}, was thus defined as:

$$F_{\text{resp}} = \sum_{i=1}^{2} |\Omega_2^{Calc} - \Omega_2^{Exp}| + |\Omega_4^{Calc} - \Omega_4^{Exp}| \quad (5)$$

where i runs over the Sparkle/PM3 and crystallographic geometries, Ω_2^{Calc} and Ω_4^{Calc} correspond to the intensity parameters calculated for each structure, and Ω_2^{Exp} and Ω_4^{Exp} to the intensity parameters obtained from the collected emission spectra. As stated above, the Ω_6 parameter was not considered in the minimization procedure because it is not observed experimentally. All values were found to be in the range of those physically acceptable.

Energy Transfer Rates. The theoretical procedure adopted to describe the energy transfer processes between the ligands and the lanthanide ion was developed by Malta and collaborators.[53−54] According to their model, the energy transfer rates, W_{ET}, can be inferred from the sum of two terms:

$$W_{ET} = W^{mm}_{ET} + W^{em}_{ET} \quad (6)$$

where W^{mm}_{ET} corresponds to the energy transfer rate obtained from the multipolar mechanism, and given by:

$$W^{mm}_{ET} = \frac{2\pi}{\hbar} \frac{e^2 S_L}{(2J + 1)G} F \sum_\lambda \gamma_\lambda \langle \alpha' J' \| U^{(\lambda)} \| \alpha J \rangle^2 + \frac{2\pi}{\hbar} \frac{e^2 S_L}{(2J + 1)G\, R_L^6} F \sum_\lambda \Omega^{e.d.}_\lambda \langle \alpha' J' \| U^{(\lambda)} \| \alpha J \rangle^2 \quad (7)$$

where G is the degeneracy of the ligand initial state and α specifies a given 4f spectroscopic term, J is the total angular momentum quantum number of the lanthanide ion. The R_L parameter (eq 7) has been calculated by:

$$R_L = \frac{\sum_i c_i^2 R_{L,i}}{\sum_i c_i^2} \quad (8)$$

with c_i being the molecular orbital coefficient of the atom i contributing to the ligand state (triplet or singlet) involved in the energy transfer, and $R_{L,i}$ corresponding to the distance from atom i to the Eu^{3+} ion.

The second term of the eq 6, W^{em}_{ET}, corresponds to the energy transfer rate obtained from the exchange mechanism. This term is calculated by:

$$W^{\text{em}}_{\text{ET}} = \frac{8\pi}{3\hbar} \frac{e^2 (1 - \sigma_0)^2}{(2J + 1) R_L^4} \times F \langle \alpha' J' \| S \| \alpha J \rangle^2 \sum_m |\langle \phi | \sum_k \mu_Z(k) s_m(k) | \phi' \rangle|^2 \quad (9)$$

where S is the total spin operator of the lanthanide ion, μ_Z is the z component of the electric dipole operator and s_m ($m = 0$, ± 1 is a spherical component of the spin operator (both for the ligand electrons), and σ_0 is a distance-dependent screening factor.[51]

The quantities F and γ_λ are given by:

$$F = \frac{1}{\hbar \gamma_L} \sqrt{\frac{\ln 2}{\pi}} \exp\left[-\left(\frac{\Delta}{\hbar \gamma_L} \right)^2 \ln 2 \right] \quad (10)$$

where γ_L is the ligand state bandwidth-at-half-maximum, and Δ is the transition energy difference between the donor and acceptor involved in the transfer process.

$$\gamma_\lambda = (\lambda + 1) \frac{\langle r^\lambda \rangle^2}{(R_L^{\lambda+2})^2} \langle 3 \| C^{(\lambda)} \| 3 \rangle^2 (1 - \sigma_\lambda)^2 \quad (11)$$

The $\langle r^\lambda \rangle$ quantity is the expected radial value of r^λ for 4f electrons (eq 11), $\langle 3 \| C^{(\lambda)} \| 3 \rangle$ is a reduced matrix element of the Racah tensor operator $\boldsymbol{C}^{(\lambda)}$,[45,55] and the σ_λ are screening factors due to the 5s and 5p filled sub-shells of the lanthanide ion.

Branching Ratios and Radiative Decay Rate. The fluorescence branching ratio, β_{0J}, consisting of the relative contribution of each $^5D_0 \rightarrow {}^7F_J$ transition to the emission spectrum, can be quantified as the ratio of the area of each band to the sum of areas of the all bands in the experimental emission spectrum. This quantity can be estimated using the Judd-Ofelt theory:[45]

$$\beta_{0,J} = \frac{A_{0,J}}{A_{Rad}} \quad (12)$$

where $A_{0,J}$ is the spontaneous emission of the each band and A_{rad} is the experimental radiative decay rates.

The $^5D_0 \rightarrow {}^7F_1$ transition can be considered as reference because it is independent of the chemical environmental, and therefore it is used in the calculus of the A_{0J} (where $J = 2$ and 4) and other intensity parameters. The spontaneous emission coefficient A_{01} is determined from emission spectra and can be estimated according to:[52]

$$A_{01} = 0.31 \times 10^{-11} \times \eta^3 \times (\sigma_1)^3 \quad (13)$$

The experimental radiative rate of the spontaneous emission, A_{rad}, can be determined by summing of the all spontaneous contributions. For this purpose, each spontaneous emission coefficient A_{02} and A_{04} is obtained from:[56]

$$A_{0J} = A_{01} \sum_J S_{0J} \times \sigma_1 / S_{01} \times \sigma_J \quad (14)$$

where S_{01} and S_{0J} are the integrated intensities of the $^5D_0 \rightarrow {}^7F_1$ and $^5D_0 \rightarrow {}^7F_J$ ($J = 2$ and 4) transitions, and σ_{01} and σ_{0J} are their barycentered energies, respectively.

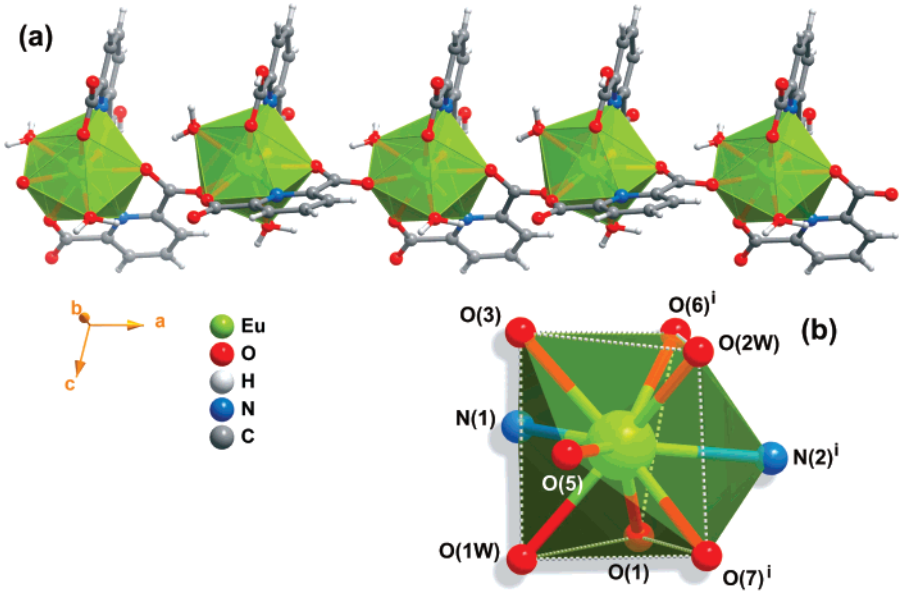

Figure 1. (a) Perspective view of the 1D $_{\infty}^{1}$[Eu(DPA)(HDPA)(H_2O)$_2$] coordination polymer running along the [100] direction of the unit cell. (b) Schematic representation of the distorted tricapped trigonal prismatic coordination environment of the crystallographically independent Eu^{3+} center. Symmetry transformation used to generate equivalent atoms: (i) $^1/_2 + x$, $^1/_2 - y$, z.

TABLE 1: Spherical Atomic Coordinates for the Single-Crystal X-ray and Sparkle/PM3 (Inside the Parentheses) {EuN_2O_7} Coordination Polyhedron, Unsigned Deviation Obtained for the Lanthanide-Coordinated-Atom Distances, Charge Factors (g) and the Polarizability (α) of the Coordinated Atom

atom	R (Å)	θ (degree)	φ (degree)	unsigned deviation	g^a	α^a
Eu	0.000 (0.000)	0.000 (0.000)	0.000 (0.000)	**0.000**		
O	2.459 (2.459)	9.000 (19.153)	99.879 (129.115)	**0.000**	0.74	2.42
O	2.509 (2.486)	119.852 (139.906)	223.790 (226.316)	**0.023**	0.74	2.42
N	2.563 (2.486)	60.326 (79.589)	204.908 (228.174)	**0.077**	2.08	0.01
O	2.507 (2.461)	87.463 (91.071)	142.119 (146.336)	**0.046**	0.74	2.42
O	2.436 (2.470)	146.482 (127.018)	333.225 (344.470)	**0.034**	0.74	2.42
N	2.564 (2.582)	147.440 (133.418)	120.821 (97.443)	**0.018**	2.08	0.01
O	2.439 (2.469)	75.275 (61.155)	359.611 (358.940)	**0.030**	2.00	6.49
O	2.434 (2.475)	86.136 (59.874)	70.491 (72.742)	**0.041**	1.59	0.23
O	2.399 (2.465)	76.870 (109.035)	285.642 (306.221)	**0.066**	1.59	0.23

[a] Obtained using a nonlinear minimization technique.

TABLE 2: Theoretical Intensity Parameters Ω_2, Ω_4, Ω_6, Radiative (A_{rad}) and Nonradiative (A_{nrad}) Decay Rates, Quantum Efficiency (η) and Quantum Yield (q) Values Derived from the Single-Crystal X-ray Diffraction and Optimized Sparkle/PM3 Models Where Related Experimental Data, Including the Lifetime (τ) of the Eu^{3+} Center, Were Obtained at Ambient Temperature for the As-Synthesized [Eu(DPA)(HDPA)(H_2O)$_2$]·4H_2O Material

	Ω_2 (10^{-20}cm^2)	Ω_4 (10^{-20}cm^2)	Ω_6 (10^{-20}cm^2)	A_{rad} (s^{-1})	A_{nrad} (s^{-1})	τ (ms)	η (%)	q (%)
experimental data	4.32	1.51		211.84	1454.80	0.6	12.7	12.0
X-ray structure	4.31	2.18	6.53	217.10	1449.54		13.0	12.5
Sparkle/PM3 structure	4.32	1.52	12.10	211.74	1454.90		12.7	12.5

The lifetime (τ) of the excited state $^5D_0$ was determined from single-exponential fittings of decay curves and is consistent with the presence of a single crystallographically independent Eu^{3+} center (see crystallographic details). The experimental set up used for these lifetime measurements comprises a Nd:YAG (third harmonic) coherent laser with $\lambda = 355$ nm used as the excitation source (frequency of 5 Hz and pulse width of 7 ns), a Tektronix TDS a 1012 oscilloscope and a fast detector ET 2000. The experimental arrangement used for lifetime measurements is presented in Figure S4 of Supporting Information.

The experimental nonradiative rate A_{nrad} is determined from:

$$\tau^{-1} = A_{rad} + A_{nrad} \quad (15)$$

The theoretical fluorescence branching ratio is similar to the spontaneous emission probability (A) of the transition and can be obtained from the Einstein coefficient to express the rate of relaxation from an excited state $^5D_0$ to a final state ^7F_J, with $J = 0-6$. The spontaneous emission probability taking into account both the magnetic dipole mechanisms and the forced electric dipole is then given by:

$$A(^5D_0 - {}^7F_J) = \frac{64\pi^4\nu^3}{3h(2J+1)}\left[\frac{n(n^2+2)^2}{9} S_{ed} + n^3 \cdot S_{md}\right] \quad (16)$$

where ν is the energy gap between the $^5D_0$ and ^7F_J states (in cm^{-1}), h is Planck's constant, $2J + 1$ is the degeneracy of the initial state, and n is the refractive index of the medium. S_{ed} and S_{md} are the electric and magnetic dipole strengths, respectively. S_{ed} is given by:

$$S_{ed} = e^2 \cdot \sum_{\lambda=2,4,6} \Omega_\lambda |\langle {}^5D_0 || U^{(\lambda)} || {}^7F_J \rangle|^2 \quad (17)$$

The $^5D_0 \rightarrow {}^7F_J$ transitions ($J = 0$, 3, and 5) are forbidden in the magnetic and induced electric dipole schemes, that is, their

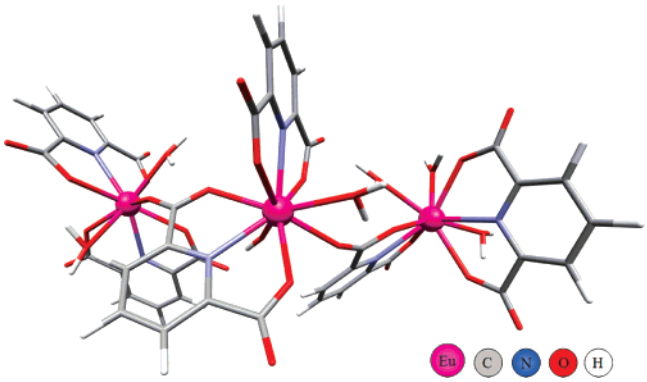

Figure 2. Optimized molecular structure of $_\infty^1$[Eu(DPA)(HDPA)-(H$_2$O)$_2$] obtained from the Sparkle/PM3 model.

strengths are taken as zero. The $^5D_0 \rightarrow {}^7F_1$ is the only transition which does not have electric dipole contribution and can be theoretically determined: $S_{md} = 9.6 \times 10^{-42}$ esu^2·cm^2.[58]

Therefore, the theoretical radiative decay rate (A_{rad}) of eq 15 is ultimately calculated as the sum of all individual spontaneous emission coefficient for the $^5D_0 \rightarrow {}^7F_{0,1,2,4}$ transitions:

$$A_{rad} = \sum_{J=1}^{6} A(^5D_0 - {}^7F_J) \tag{18}$$

The emission quantum efficiency η can be expressed as

$$\eta = \frac{A_{rad}}{A_{rad} + A_{nrad}} \tag{19}$$

The numerical solution of the rate equations describing the kinetics of the 4f−4f luminescence was carried out according to the model developed by Malta and collaborators, [55] thus yielding the time dependence of the energy level populations, which reach the steady-state regime after 10^{-6}−10^{-5} s. These steady-state populations were further used to calculate the emission quantum yield given by:

$$q = \frac{A_T \eta_2}{\phi \eta_1} \tag{20}$$

where the sub-indices 1 and 2 indicate the ground state and the emitting level of the complex, A_T corresponds to the sum of the coefficients of spontaneous emission for the $^5D_0 \rightarrow {}^7F_{0,1,2,4}$ transitions and ϕ is the pumping rate.

Results and Discussion

Crystal Structure and Sparkle/PM3 Geometry Prediction. The structure of [Eu(DPA)(HDPA)(H$_2$O)$_2$]·4H$_2$O contains a single crystallographically independent Eu^{3+} cation bound to two H$_{2-x}$DPA^{x-} residues (where $x = 1, 2$) which exhibit slightly distinct coordination fashions (Figure 1a), even though both the mono-deprotonated, HDPA$^-$, and the fully deprotonated, DPA^{2-}, residues are anti,anti-chelated to the lanthanide; one carboxylate group from the latter residue further establishes a syn-bridge with a symmetry-related Eu^{3+} cation, imposing a Eu···Eu^i separation of 6.497[1] Å [symmetry transformation: (i) $1/2 + x$, $1/2 - y$, z]. This leads to the formation of a neutral one-dimensional coordination polymer, $_\infty^1$[Eu(DPA)(HDPA)(H$_2$O)$_2$] (Figure 1a), running parallel to the [100] direction of the unit cell. The coordination sphere of Eu^{3+} also comprises two water molecules and can be best described as a distorted tricapped trigonal prism, {EuN$_2$O$_7$} (Figure 1b), with local C_{2v} symmetry

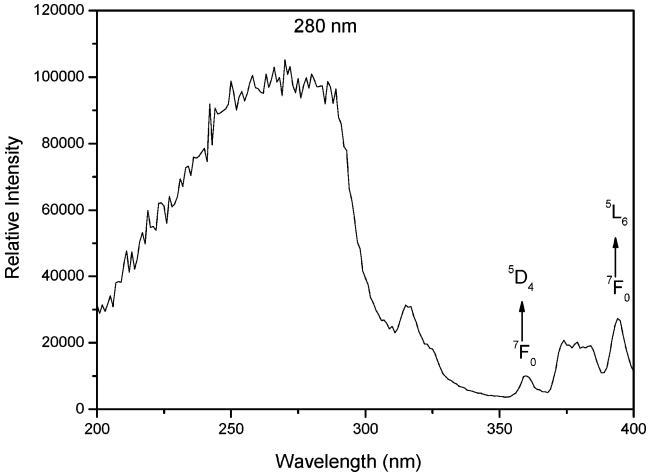

Figure 3. Excitation spectra of [Eu(DPA)(HDPA)(H$_2$O)$_2$]·4H$_2$O recorded at 300 K by monitoring emission of Eu^{3+} at 615 nm.

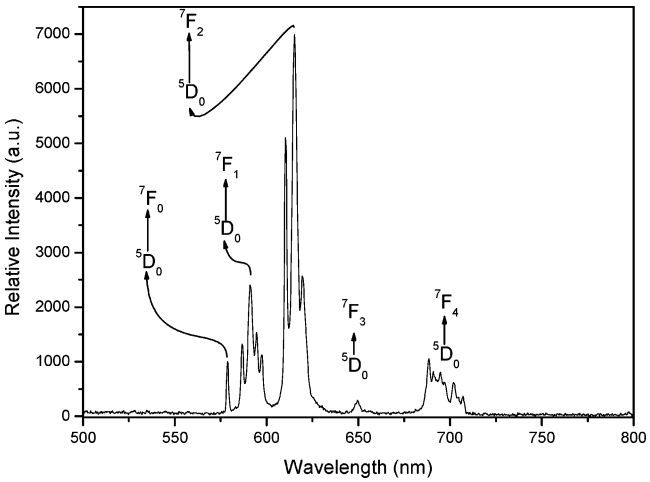

Figure 4. Emission spectrum of [Eu(DPA)(HDPA)(H$_2$O)$_2$]·4H$_2$O recorded at 77K and upon excitation at 280 nm.

which deviates from the typical D_3 reported for similar compounds.[59] The registered Eu−O bond lengths were found in the 2.394(2)−2.508(2) Å range, and the two Eu−N are identical and of 2.564(2) Å. These values are well within the expected ranges found for similar compounds in which Eu^{3+} coordinated to H$_2$DPA residues,[38,60−64] while the Eu−O bond lengths are usually in the 2.40−2.51 Å range (median of 2.45 Å), the Eu−N distances are instead in the 2.49−2.57 Å range (median of 2.54 Å).

Spherical atomic coordinates for the crystallographic and Sparkle/PM3 {EuN$_2$O$_7$} coordination polyhedra are summarized in Table 1, with the optimized geometry obtained from the Sparkle/PM3 model being represented in Figure 2. It is important to emphasize that the Sparkle/PM3 model agrees well with the data derived from the crystallographic studies, with the minimized Eu···Eu internuclear distance across the chain being of 6.694 Å, and the Eu−O and Eu−N distances found in the 2.459−2.486 Å and 2.582−2.584 Å ranges, respectively. This good agreement between the two structural models is further supported by an unsigned average error of only 0.037 Å (Table 1).

Thermal Analysis. In Figure S5 of Supporting Information, there are presented the TG/DTG curves recorded in dynamic nitrogen atmosphere. The thermal decomposition of [Eu(DPA)-(HDPA)(H$_2$O)$_2$]·4H$_2$O develops in three consecutive stages. The average of first weight loss of approximately 15.3% occurs in the 40−190 °C temperature range and is attributed to the release

TABLE 3: Calculated Values of Intramolecular Energy Transfer and Back-Transfer Rates in [Eu(DPA)(HDPA)$(H_2O)_2$·$4H_2O$] Polymer

	singlet → $^5D_4$		triplet → $^5D_1$		triplet → $^5D_0$	
	W_{ET1}[a] (s^{-1})	W_{BT1}[b] (s^{-1})	W_{ET2}[a] (s^{-1})	W_{BT2}[b] (s^{-1})	W_{ET3}[a] (s^{-1})	W_{BT3}[b] (s^{-1})
X-ray structure	2.13×10^4	0.00	2.39×10^7	4.72	8.98×10^6	3.85×10^{-4}
Sparkle/PM3 structure	1.88×10^4	1.92×10^{-13}	1.13×10^8	2.93×10^2	4.82×10^7	2.70×10^{-2}

[a] W_{ET}, transfer rate. [b] W_{BT}, back-transfer rate.

of uncoordinated water molecules housed in the channels (calculated value for five water molecules of *ca.* 15.2%). Decomposition of the dehydrated phase proceeds with two further weight losses to give a residue (*ca.* 32.4%) attributed to the formation of the stoichiometric amount of Eu_2O_3 (calculated residue of *ca.* 29.8%). DSC measurements agree well with the thermogravimetric behavior, with a deep and broad endothermic peak being registered in the 58−99 °C temperature range. Noteworthy is the fact that DSC further shows that no other phase transition is registered up to approximately 400 °C at which time thermal decomposition of the organic component starts to settle in. This is a clear indication that the dehydrated material is indeed stable up to this temperature.

Photophysical Properties. The excitation spectra of [Eu(DPA)(HDPA)$(H_2O)_2$]·$4H_2O$ was registered in the 200−400 nm range by monitoring the emission of Eu^{3+} at 615 nm, and it is showed in Figure 3. The [Eu(DPA)(HDPA)$(H_2O)_2$]·$4H_2O$ excitation exhibits a broad band between 200 and 310 nm (λ_{max} = 280 nm) from $\pi \rightarrow \pi^*$ electronic transition of the ligand. The peaks observed in the 310−400 nm range result from the f−f transitions of the Eu^{3+} ion, and they are very weak in comparison to the ligand absorption. It is clearly indicate that a typical antenna effect involving the organic ligand is the most probable photophysical pathway responsible for the luminescence of the sample.

Figure 4 shows the emission spectra recorded in the 500−720 nm range, displaying the typical narrow bands corresponding to the centered Eu^{3+} $^5D_0 \rightarrow {}^7F_J$ transitions, with the main emission centered at approximately 615 nm and corresponding to the $^5D_0 \rightarrow {}^7F_2$ transition. The relative intensities and splitting of the emissions bands are particularly influenced by symmetry of the first coordination sphere.

The emission spectrum has a single peak at approximately 578 nm attributed to the $^5D_0 \rightarrow {}^7F_0$ transition, which remains unaltered once the temperature is lowered to 77 K. This clearly indicates the presence of a single Eu^{3+} center, which in good agreement with the crystallographic and Sparkle/PM3 models (see section dedicated to crystal description). Selection rules for the electric dipole transition indicate that the $^5D_0 \rightarrow {}^7F_0$ is only observed if the point symmetry of Eu^{3+} is either C_{nv}, C_n or C_s,[67] again in accord with the structural models presented above. The $^5D_0 \rightarrow {}^7F_1$ transition, which is ruled by a magnetic dipole mechanism and being largely independent of the ligand field effects, exhibits four well-defined Stark components, thus supporting the presence of a low site symmetry for Eu^{3+}.[68] The presence of a fourth emission line on the $^5D_0 \rightarrow {}^7F_1$ transition can be attributed to electron/phonon coupling, caused by noncoordinated water molecules, delocalized from equilibrium position after the decreasing temperature.[10] Moreover, the $^5D_0 \rightarrow {}^7F_2/{}^5D_0 \rightarrow {}^7F_1$ ratio for [Eu(DPA)(HDPA)$(H_2O)_2$]·$4H_2O$ is of approximately 2.8, which is considerably higher than 0.67 typical of europium center exhibiting centrosymmetric.[69] The emission spectrum, at 300 K, of the coordination polymer is presented in Supporting Information (Figure S6).

Table 2 summarizes the theoretical (derived from the expression depicted in Experimental Section) and experimental values for the intensity parameters (Ω_2, Ω_4, and Ω_6 radiative and nonradiative rates of spontaneous emission (A_{rad} and A_{nrad}, respectively), quantum efficiency (η) and yield (q), and experimental lifetime (τ) for [Eu(DPA)(HDPA)$(H_2O)_2$]·$4H_2O$. The short lifetime of 0.6 ms can be directly associated to the nonradiative decay channels controlling the relaxation process (see Table 2) and arising from the vibronic coupling with the water molecules present in the structure. Indeed, it is well-known that O−H oscillators are the most effective quenchers of the Eu^{3+} excited state, both in solution and in the solid state.[71,72] This quenching effect is particularly important in the solid state, with even uncoordinated water molecules can contribute to the overall effect. For example, the single uncoordinated water molecule in compound [Eu$(oda)_3$]·H_2O (oda = oxidiacetate), located at 5.05 Å from the optical center, has an astonishing rate of contribution to the overall quenching of 260 s^{-1}.[73] Since in [Eu(DPA)(HDPA)$(H_2O)_2$]·$4H_2O$ two of the four crystallographically independent water molecules of crystallization have an effective distance to the lanthanide center smaller than 5.0 Å, it is thus feasible to assume that the same effect can also occur in the material in study. Therefore, the water clusters have a dual structural function: while on the one hand they stabilize the supramolecular framework of [Eu(DPA)(HDPA)$(H_2O)_2$]·$4H_2O$, on the other they also constitute a nonradiative channel. Indeed, this later function provides a plausible explanation for the observed short lifetime and experimental radiative rate (A_{rad} = 211.84 s^{-1}), the high value for experimental nonradiative rate (A_{nrad} = 1454.83 s^{-1}) and the low experimental quantum efficiency (η = 12.7%). These results are also consistent with the theoretical considerations proposed by Föster and Dexter,[74,75] which predict that the probability of energy transference scales to $1/R^6$, where R is the distance between the donor and the acceptor (the water cluster in this case).

The theoretical intensity parameters Ω_λ (λ = 2, 4, and 6) calculated using the Sparkle/PM3 and crystallographic models are summarized in Table 2. The theoretical values are in excellent agreement with those obtained experimentally. It is worth mentioning that the values for Ω_2 are relatively small when compared with those of Eu-β-diketonates.[76] This is a clear indication of a reduced degree of covalence involving the metal−ligand coordination bond and also of a slightly polarizable chemical environment for the lanthanide center.[77−79]

The ligand-to-metal energy transfer may occur through either the singlet or triplet ligand states. The energies of the triplet and singlet states calculated for the crystallographic structure using the INDO/CIS method are 22 313.7 cm^{-1} and 37 126.6 cm^{-1}, respectively. The same physical quantities obtained using the Sparkle/PM3 structure are 21 774.3 cm^{-1} and 35 812.3 cm^{-1}, respectively. As clearly depicted in Figure 5, the singlet state of the $_\infty{}^1$[Eu(DPA)(HDPA)$(H_2O)_2$] coordination polymer does not have appropriate resonance conditions with the europium trivalent ion. Thus, we decided to consider the singlet → $^5D_4$ channel in all our calculations. The parameters needed to calculate the energy transfer rates and emission quantum yield have been obtained from the Sparkle/PM3 and X-ray structures and from spectroscopic calculations.

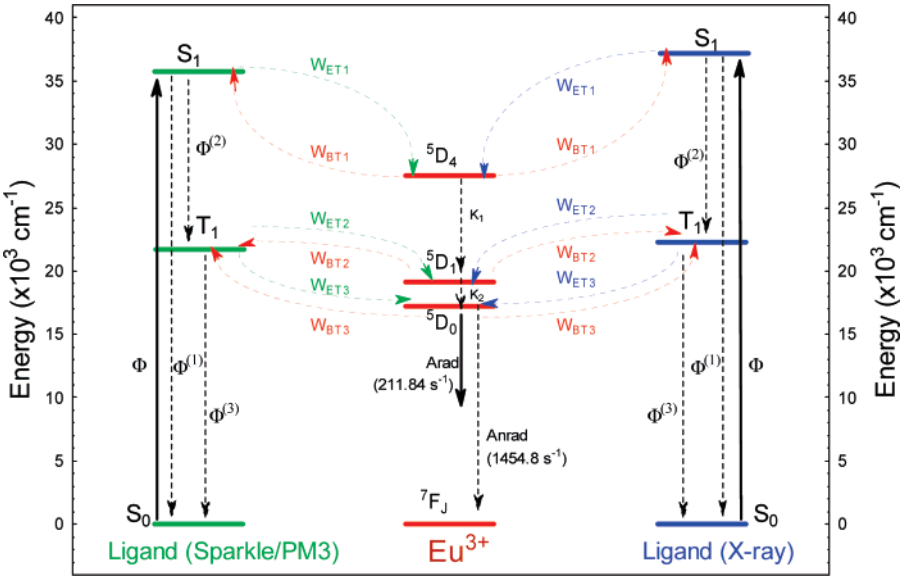

Figure 5. Energy level diagram for [Eu(DPA)(HDPA)(H$_2$O)$_2$]·4H$_2$O showing the most probable channels for the intramolecular energy transfer process.

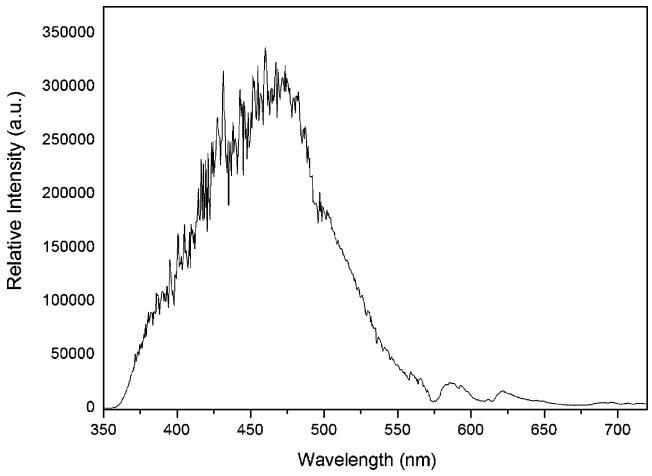

Figure 6. Emission spectrum of [Gd(DPA)(HDPA)(H$_2$O)$_2$]·4H$_2$O recorded at 77K and upon excitation at 280 nm.

The triplet state of the ligand was determined from the phosphorescence spectrum at 77 K from Gd compound. Since Gd^{3+} has no energy levels below 32 000 cm^{-1}, it cannot accept energy from the ligand triplet state. The triplet state energy was estimated from shortest-wavelength phosphorescence band, which was assumed as being 0−0 transition.[80] The Figure 6 shows the low-temperature phosphorescence spectrum of the Gd compound obtained in the range 370−720 nm when excited at 340 nm. As can be observed from Figure 6, the triplet state is centered at 460 nm (21 740 cm^{-1}), whose the theoretical values are in good agreement.

The energy transfer rates are larger for those levels dominated by the exchange mechanism, $^5D_0$ and $^5D_1$, than for those dominated by the dipole−dipole. Typical values of the remaining transfer rates were assumed to be identical to those found for coordination compounds, namely, $\Phi = 10^4$, $\Phi^{(1)} = 10^6$, $\Phi^{(2)} = 10^8$, and $\Phi^{(3)} = 10^5$ s^{-1}.[54] The energy transfer rates from the ligand triplet state (T1) to the $^5D_1$ and $^5D_0$ levels and energy transfer rates from the singlet state (S1) to the $^5D_4$ level are summarized in Table 3. Clearly, the values of the energy transfer rate indicate it is predominant from the triplet state of the ligand to the $^5D_1$ and $^5D_0$ levels of the Eu^{3+} ion.

The comparison between branching ratio, β_{0J}, values for the $^5D_0 \rightarrow {}^7F_J$ transitions obtained from experimental spectrum

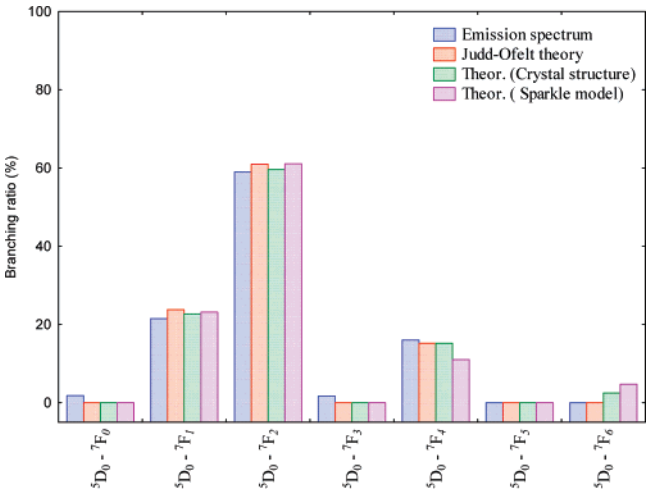

Figure 7. Data comparison for emission spectra of [Eu(DPA)(HDPA)-(H$_2$O)$_2$]·4H$_2$O, expressed by branching ratios β_{OJ}.

emission, with those estimated from the Judd-Ofelt theory and also those theoretically calculated the from crystallographic and simulated Sparkle/PM3 models is represented in Figure 7. As expected, the theoretical values are in very good agreement with those obtained experimentally.

The lifetime value (τ) of the $^5D_0$ level, the radiative (A_{rad}) and nonradiative (A_{nrad}) rates used in the quantum yield calculations, plus the theoretical quantum yields (derived from the Sparkle/PM3 and crystallographic structural models) are all given in Table 2. Notably, all values for the latter physical property are in perfect agreement with each other.

Conclusions

We have successfully reacted H$_2$DPA with Eu^{3+} under typical hydrothermal conditions to produce a photoluminescent material, [Eu(DPA)(HDPA)(H$_2$O)$_2$]·4H$_2$O, whose crystal structure was elucidated by single-crystal X-ray crystallography and showed to be composed by one-dimensional $_\infty{}^1$[Eu(DPA)(HDPA)-(H$_2$O)$_2$] coordination polymers, mutually interacting via an extensive hydrogen-bonding network composed of water clusters. The optimized molecular geometry for this material was obtained by employing the Sparkle/PM3 model, and shows a

very good agreement with crystallographic structure, thus rendering this in silico approach as a new and more efficient alternative over the traditional concepts used in the investigation of coordination polymers containing lanthanides ions.

The intensity parameters acquired experimentally (from emission spectra) are in excellent agreement with those calculated from both crystallographic and Sparkle/PM3 structures. The values of Ω_2 denote low covalent nature of the metal−ligand bonds thus showing that chemical environment around the Eu^{3+} metallic center is slightly polarizable. This observation was further confirmed by using the intensity ratio $^5D_0 \rightarrow {}^7F_2/{}^5D_0 \rightarrow {}^7F_1$. Values for the intermolecular energy transfer rate indicate that the energy transfer is predominant from the triplet state of the ligand to the $^5D_1$ and $^5D_0$ levels of the Eu^{3+} ion. The small values calculated for the quantum efficiency, lifetime and quantum yield can be directly associated with nonradiative decay channels controlling the relaxation process of $^5D_0$ level, namely, the presence of water clusters which provide a structurally important source of O−H oscillators.

The calculated quantum yields obtained from the crystallographic and Sparkle/PM3 structural models (both of about 12.5%) are in good agreement with the experimental value (12.0 ± 5%). These results, associated with the excellent predictions of the intensity parameters, radiative rate, and quantum efficiencies certify the efficacy of the theoretical models used in all calculations and open new and interesting possibilities for the design in silico of highly efficient lanthanide−organic frameworks.

Acknowledgment. We kindly thank the financial support from CNPq (Brazilian agency) through of the PADCT and for the research grants from the Instituto do Milênio de Materiais Complexos. We also wish to thank CENAPAD (Centro Nacional de Processamento de Alto Desempenho) at Campinas, Brazil, for providing access to their computational facilities.

Supporting Information Available: Discussions about the crystallographic characterization of the compound. Additional drawings showing the TG/DTG curves; experimental setup used to measure the lifetimes of $[Eu(DPA)(HDPA)(H_2O)_2]\cdot 4H_2O$; a comparison between the FT-IR spectra of $[Eu(DPA)(HDPA)(H_2O)_2]\cdot 4H_2O$ and H_2DPA and emission spectra of $[Eu(DPA)(HDPA)(H_2O)_2]\cdot 4H_2O$ recorded at 300 K. This material is available free of charge via the Internet at http://pubs.acs.org.

References and Notes

(1) Bettencourt-Dias, A. *Inorg. Chem.* **2005**, *44*, 2734−2741.
(2) Mueller, U.; Schubert, M.; Teich, F.; Puetter, H.; Schierle-Arndt, K.; Pastré, J. *J. Mater. Chem.* **2006**, *16* (7), 626−636.
(3) Grant, A. B.; Marc, A. K.; Robin, D. R. *J. Alloys Comp*. **2002**, *344*, 123−127.
(4) Pan, L.; Huang, X.; Li, J.; Wu, Y.; Zeng. N. *Angew. Chem., Int. Ed*. **2000**, *39*, 527−530.
(5) Hifumi, H.; Yamaoka, S.; Tanimoto, A.; Citterio, D.; Suzuki, K. *J. Am. Chem. Soc.* **2006**, *128*, 15090−15091.
(6) Viswanathan, S.; Bettencourt-Dias, A. *Inorg. Chem.* **2006**, *45*, 10138−10146.
(7) Parvithran, R.; Kumar, N. S. S.; Biju, S.; Reddy, M. L. P.; Junior, S. A.; Freire, R. O. *Inorg. Chem.* **2006**, *45*, 2184−2192.
(8) Alpha, B.; Ballardinni, R.; Balzani, V.; Lehn, J. M.; Perathoner, S.; Sabbatini, N. *Angew. Chem., Int. Ed*. **1987**, *26*, 1266−1267.
(9) Shi, Q.; Zhang, S.; Wang, Q.; Ma, H.; Yang, G.; Sun, W. S. *J. Mol. Struct.* **2007**, *837*, 185−189.
(10) Choppin, G. R.; Bünzli, J. C. G. *Lanthanides Probes in Life Chemical and Earth Sciences Theory and Practice;* Elsevier: Amsterdam, 1989.
(11) Richardson, F. S. *Chem. Rev.* **1982**, *82*, 541−552.
(12) Kido, J.; Okamoto, Y. *Chem. Rev*. **2002**, *102*, 2357−2368.
(13) Zhao, B.; Chen, X. Y.; Cheng, P.; Liao, D. Z.; Yan, S. P.; Jiang, Z. H. *J. Am. Chem. Soc.* **2004**, *126*, 15394−15395.
(14) Wang, F. Q.; Zheng, X. J.; Wan, Y. H.; Sun, C. Y.; Wang, Z. S.; Wang, K. Z.; Jin, L. P. *Inorg. Chem.* **2007**, *46*, 2956−2958.
(15) Qin, C.; Wang, X. L.; Wang, E. B.; Su, Z. M. *Inorg. Chem.* **2005**, *44*, 7122−7129.
(16) Meskers, S. C. J.; Ubbink, M.; Canters, G. W.; Dekkers, H. P. J. M. *J. Phys. Chem.* **1996**, *100*, 17957−17969.
(17) Liu, M.; Zhao, L.; Lin, J. M. *J. Phys. Chem. A* **2006**, *110*, 7509−7514.
(18) Zhao, B.; Yi, L.; Dai, Y.; Chen, X. Y.; Cheng, P.; Liao, D. Z.; Yan, S. P.; Jiang, Z. H. *Inorg. Chem.* **2005**, *44*, 911−920.
(19) Fernades, A.; Jaud, J.; Dexpert-Ghys, J.; Brouca-Cabarrec, C. *Polyhedron* **2001**, *20*, 2385−2391.
(20) Brayshaw, P. A.; Hall, A. K.; Harrison, W. T. A.; Harrowfield, J. M.; Pearce, D.; Shand, T. M.; Skelton, B. W.; Whitaker, C. R.; White, A. H. *J. Eur. Inorg. Chem.* **2005**, 1127−1141.
(21) Mellot-Draznieks, C.; Férey, G. *Prog. Solid State Chem.* **2005**, *33*, 187−197.
(22) Dolg, M.; Stoll, H.; Savin, A.; Preuss, H. *Theor. Chim. Acta* **1989**, *75*, 173−194.
(23) Cundari, T. R.; Stevens, W. *J. Chem. Phys.* **1993**, *98*, 5555−5565.
(24) Dolg, M. *In Modern Methods and Algorithms of Quantum Chemistry*; Grotendorst, J., ed.; John von Neumann Institute for Computing, Jülich, NIC series, 2000, *1*, 479.
(25) Freire, R. O.; Rocha, G. B.; Simas, A. M. *Inorg. Chem.* **2005**, *44*, 3299−3310.
(26) Freire, R. O.; Rocha, G. B.; Simas, A. M. *J. Mol. Model.* **2006**, *12*, 373−389.
(27) Freire, R. O.; Rocha, G. B.; Albuquerque, R. Q.; Simas, A. M. *J. Lumin.* **2005**, *111*, 81−87.
(28) Albuquerque, R. Q.; Freire, R. O.; Malta, O. L. *J. Phys. Chem. A* **2005**, *109*, 4607−4610.
(29) Beltrão, M. A.; Santos, M. L.; de Mesquita, M. E.; Barreto, L. S.; Júnior, N. B. C.; Freire, R. O.; dos Santos, M. A. C. *J. Lumin.* **2006**, *116*, 132−138.
(30) da Costa, N. B.; Freire, R. O.; dos Santos, M. A. C.; de Mesquita, M. E. *J. Mol. Struct. (Theochem*) **2001**, *545*, 131−135.
(31) de Mesquita, M. E.; Junior, S. A.; Oliveira, F. C.; Freire, R. O.; Júnior, N. B. C.;de Sá, G. F. *Inorg. Chem. Commun.* **2002**, *5*, 292−295.
(32) Mesquita, M. E.; Junior, S. A.; Júnior, N. B. C.; Freire, R. O.; Silva, F. R. G.; Sá, G. F. *J. Solid State Chem.* **2003**, *171*, 183−188.
(33) de Mesquita, M. E.; Gonçalves e Silva, F. R.; Albuquerque, R. Q.; Freire, R. O.; da Conceição, E. C.; da Silva, J. E. C.; Júnior, N. B. C.; de Sá, G. F. *J. Alloys Comput.* **2004**, *366*, 124−131.
(34) Mesquita, M. E.; Junior, S. A.; Silva, F. R. G.; Couto, M. A. S.; Freire, R. O.; Júnior, N. B. C.; Sá, G. F. *J. Alloys Comput.* **2004**, *374*, 320−324.
(35) Pavithran, R.; Reddy, M. L. P.; Alves, S., Jr; Freire, R. O.; Rocha, G. B.; Lima, P. P. *Eur. J. Inorg. Chem.* **2005**, *20*, 4129−4127.
(36) Freire, R. O.; Silva, F. R. G.; Rodrigues, M. O.; Mesquita, M. E.; Júnior, N. B. C. *J. Mol. Model.* **2005**, *12*, 16−23.
(37) Freire, R. O.; Albuquerque, R. Q.; Júnior, S. A.; Rocha, G. B.; Mesquita, M. E. *Chem. Phys. Lett.* **2005**, *405*, 123−126.
(38) Brayshaw, P. A.; Hall, A. K.; Harrison, W. T. A.; Harrowfield, J. M.; Pearce, D.; Shand, T. M.; Skelton, B. W.; Whitaker, C. R.; White, A. H. *Eur. J. Inorg. Chem.* **2005**, 1127−1141.
(39) Bril, A.; De Jager-Veenis, A. W. *J. Res. Nat. Bureau Stand*. **1976**, *80A*, 401−407.
(40) Malta, O. L.; Brito, H. F.; Menezes, J. F. S.; Gonçalves e Silva, F. R.; de Mello, Donegá, C.; Alves, Jr. S. *Chem. Phys. Lett.* **1998**, *282*, 233−238.
(41) Stewart; J. J. P. *MOPAC2007*, Version 7.058; Stewart Computational Chemistry: Colorado Springs, CO, 2007.
(42) Ridley, J. E.; Zerner, M. C. *Theor. Chim. Acta* **1976**, *42*, 223−236.
(43) Zerner, M. C.; Loew, G. H.; Kirchner, R. F.; Mueller-Westerhoff, U. T. *J. Am. Chem. Soc.* **1980**, *102*, 589−599.
(44) Zerner, M. C. *ZINDO manual*, QTP, University of Florida: Gainesville, FL 32611, 1990.
(45) Judd, B. R. *Operator Techniques in Atomic Spectroscopy*, 2nd ed. McGraw-Hill Book Company: New York, 1998.
(46) Guan, J.; Chen, B.; Sun, Y.; Liang, H.; Zhang, Q. *J. Non-Cryst. Solids* **2005**, *351*, 849−855.
(47) Judd, B. R. *Phys. Rev.* **1962**, *127*, 750−761.
(48) Ofelt, G. S. *J. Chem. Phys.* **1962**, *37*, 511−520.
(49) Malta, O. L.; Ribeiro, S. J. L.; Faucher, M.; Porcher, P. *J. Phys. Chem. Solids* **1991**, *52*, 587−593.
(50) Malta, O. L.; Couto dos Santos, M. A.; Thompson, L. C.; Ito, N. K. *J. Lumin.* **1996**, *69*, 77−84.
(51) Malta, O. L.; Brito, H. F.; Meneses, J. F. S.; e Silva, F. R. G.; Alves, S., Jr.; Farias, F. S., Jr.; de Andrade, A. V. M. *J. Lumin.* **1997**, *75*, 255−268.

(52) de Sá, G. F.; Malta, O. L.; de Mello Donegá, C.; Simas, A. M.; Longo, R. L.; Santa-Cruz, P. A.; da Silva, E. F., Jr. *Coord. Chem. Rev.* **2000**, *196*, 165−195.
(53) Malta, O. L.; e Silva, F. R. G. *Spectrochim. Acta Part A* **1998**, *54*, 1593−1599.
(54) Malta, O. L.; e Silva, F. R. G.; Longo, R. *Chem. Phys. Lett.* **1999**, *307*, 518−526.
(55) Carnall, W. T.; Crosswhite, H.; Crosswhite, H. M. *Energy Structure and Transition Probabilities of the Trivalent Lanthanides in LaF3*; Argonne National Laboratory Report; unnumbered, 1977.
(56) Araujo, A. A. S.; Brito, H. F.; Malta, O. L.; Matos, J. R.; Teotônio, E. E. S.; Storpirtis, S.; Izumi, C. M. S. *J. Ionrg. Biochem.* **2002**, *88*, 87−93.
(57) Van Deun, R.; Binnemans, K.; Görrler-Walrand, C.; Adam, J. L. *J. Phys. Condens. Matter* **1998**, *10*, 7231−7241.
(58) Weber, M. J.; Varitimos, T. E.; Matsinger, B. H. *Phys. Rev. B* **1973**, *8*, 47−53.
(59) Brayshaw, P. A.; Bünzli, J. C. G.; Froidevaux, P.; Harrowfield, J. M.; Kim, Y.; Sobelev, A. N. *Inorg. Chem.* **1995**, *34*, 2068−2076.
(60) Zhao, B.; Chen, X. Y.; Cheng, P.; Liao, D. Z.; Yan, S. P.; Jiang, Z. H. *J. Am. Chem. Soc.* **2004**, *126*, 15394−15395.
(61) Renaud, F.; Piguet, C.; Bernardinelli, G.; Bunzli, J. C. G.; Hopfgartner, G. *Chem.-Eur. J.* **1997**, *3*, 1660−1667.
(62) Brayshaw, P. A.; Harrowfield, J. M.; Sobolev, A. N. *Acta Cryst. C* **1995**, *51*, 1799−1802.
(63) Brayshaw, P. A.; Bunzli, J. C. G.; Froidevaux, P.; Harrowfield, J. M.; Kim, Y.; Sobolev, A. N. *Inorg. Chem.* **1995**, *34*, 2068−2076.
(64) Zhou, D. J.; Huang, C. H.; Wang, K. Z.; Xu, G. X. *Polyhedron* **1994**, *13*, 987−991.
(65) Bernstein, J.; Davis, R. E.; Shimoni, L.; Chang, N. L. *Angew. Chem., Int. Edit. Engl.* **1995**, *34*, 1555−1573.
(66) Doedens, R. J.; Yohannes, E.; Khan, M. I. *Chem. Commun.* **2002**, *1*, 62−63.
(67) Binnemans, K.; Van Herck, K.; Göller-Walard, C. *Chem. Phys. Lett.* **1997**, *266*, 297−302.
(68) Bejan, C. C. C.; Rocha, G. B.; Albuquerque, R. Q.; Demnitz, F. W. J.; de Sá, G. F.; Júnior, S. A. *J. Lumin.* **2005**, *113*, 79−88.
(69) Klink, S. I.; Graves, L.; Reinhoudt, D. N.; van Veggel, F. C. J. M.; Werts, M. H. V.; Geurts, F. A. J.; Hofstraat, J. W. *J. Phys. Chem. A* **2000**, *104*, 5457−5468.
(70) Georgge, M. R.; Golden, C. A.; Grossel, M. C.; Curry, R. J. *Inorg. Chem.* **2004**, *43*, 6887−6889.
(71) Tedeschi, C.; Azéma, J.; Gornitzka, H.; Tisnès, P.; Picard, C. *J. Chem. Soc., Dalton Trans.* **2003**, *9*, 1738−1745.
(72) An, Y.; Berry, M. T.; van Veggel, F. C. J. M. *J. Phys. Chem. A* **2000**, *104*, 11243−11247.
(73) May, P. S.; Richardson, F. S. *Chem. Phys. Lett.* **1991**, *179*, 277−281.
(74) Förster, T. *Discuss. Faraday Soc.* **1959**, *27*, 7−17.
(75) Dexter, D. L. *J. Chem. Phys.* **1953**, *21*, 836−850.
(76) Lima, P. P.; Sá, F. R. A.; Freire, R. O.; Paz, F. A. A.; Fu, L.; Júnior, S. A.; Carlos, L. D.; Malta, O. L. *Chem. Phys. Chem.* **2006**, *7*, 735−746.
(77) Mesquita, M. E.; de Sá, G. F.; Malta, O. L. *J. Alloys Comput.* **1998**, *275*, 844−847.
(78) Driesen, K.; Fourier, S.; Göller-Walrand, C.; Binnemans, K. *Phys. Chem. Chem. Phys.* **2003**, *5*, 198−202.
(79) Santos, E. R.; Santos, M. A. C.; Freire, R. O.; Júnior, S. A.; Barreto, L. S.; Mesquita, M. E. *Chem. Phys. Lett.* **2006**, *418*, 337−341.
(80) Chandler, B. D.; Cramb, D. T.; Shimidzu, G. K. H. *J. Am. Chem. Soc.* **2006**, *128*, 10403−10412.